

# Experimental Realization of a Quantum Refrigerator Driven by Indefinite Causal Orders

Xinfang Nie,<sup>1,2,\*</sup> Xuanran Zhu,<sup>1,\*</sup> Cheng Xi,<sup>1</sup> Xinyue Long,<sup>1</sup> Zidong Lin,<sup>1</sup> Yu Tian,<sup>1</sup> Chudan Qiu,<sup>1</sup> Xiaodong Yang,<sup>1</sup> Ying Dong,<sup>3</sup> Jun Li,<sup>1,2,†</sup> Tao Xin,<sup>1,2,‡</sup> and Dawei Lu<sup>1,2,§</sup>

<sup>1</sup>*Shenzhen Institute for Quantum Science and Engineering and Department of Physics, Southern University of Science and Technology, Shenzhen 518055, China*

<sup>2</sup>*Guangdong Provincial Key Laboratory of Quantum Science and Engineering, Southern University of Science and Technology, Shenzhen 518055, China*

<sup>3</sup>*Research Center for Quantum Sensing, Zhejiang Lab, Hangzhou, Zhejiang, 311121, China*

(Dated: November 26, 2020)

Indefinite causal order (ICO) is playing a key role in recent quantum technologies. Here, we experimentally study quantum thermodynamics driven by ICO on nuclear spins using the nuclear magnetic resonance system. We realize the ICO of two thermalizing channels to exhibit how the mechanism works, and show that the working substance can be non-classically cooled or heated albeit it undergoes thermal contacts with reservoirs of the same temperature. Moreover, we construct a single cycle of the ICO refrigerator, and evaluate its efficiency by measuring the work consumption and the heat energy extracted from the low-temperature reservoir. Unlike classical refrigerators in which the efficiency is perversely higher the closer the temperature of the high-temperature and low-temperature reservoirs are to each other, the ICO refrigerator's efficiency of performance is always bounded to small values due to the non-unit success probability in projecting the ancillary qubit to the preferable subspace. Our experiment demonstrates that the ICO process may offer a new resource with non-classical heat exchange, and paves the way towards construction of quantum refrigerators on a quantum system.

*Introduction.* – Quantum thermodynamics, as an interdisciplinary between thermodynamics and quantum mechanics, aims to broaden the standard thermodynamics to the system dominated by quantum mechanics [1–8]. Facilitated by the development of quantum information theory and experimental techniques, quantum heat engine has been demonstrated a good platform to study quantum thermodynamics [9–19]. The idea of quantum heat engines originates from the model proposed by Szilard in 1929 [20], where the famous Maxwell's demon utilizes the information to extract work from the reservoir. Recently, apart from previous protocols, a new class of thermodynamic resources stemming from the indefinite causal order (ICO) is shown to be capable of effectively building quantum heat engines [21]. Events happen with definite order in daily experience. However, in quantum mechanics, events can happen without a fixed causal order induced by quantum superposition [22–25]. ICO is proven to yield superiorities in many research areas, including quantum computation [22, 24], communication complexity [26], metrology [27, 28], and quantum information transmission [29, 30].

The recent theoretical research [21] proposes to apply ICO in quantum thermodynamics. By projecting the ancillary qubit onto its relevant subspace, a working system can be non-classically cooled or heated with the ICO of two equivalent thermalizing channels of the same temperature. This is counterintuitive, because empirically exchanging the order of two equivalent channels would not impact on the final temperature. This exotic property comes from the magic of quantum information, leading to a new design of quantum refrigerators that only consume work by erasing the information preserved in the ancilla.

In this work, using the ensemble of nuclear spins in the nuclear magnetic resonance (NMR) system [31], we experimentally demonstrate the ICO process and refrigerators. We

show that projective measurements of the ancilla in different basis result in distinct thermodynamic performances. Moreover, we investigate the efficiency of the quantum refrigerator in one cooling cycle, and show its completely different properties from classical refrigerators.

*Theory.* – Let us briefly review the ICO-based quantum thermodynamics. A quantum channel is a completely positive trace-preserving map. In the operator-sum representation, the state of a system after undergoing a general quantum channel  $\mathcal{E}$  can be written as  $\mathcal{E}(\rho) = \sum_k E_k \rho E_k^\dagger$ , where  $\{E_k\}$  are Kraus operators satisfying  $\sum_k E_k^\dagger E_k = I$ . In thermodynamics, a thermalizing channel of temperature  $T$  transfers an arbitrary input state  $\rho$  to a thermal equilibrium state  $\rho_T$  at temperature  $T$ . This thermalizing channel can be described by a quantum depolarizing channel [32]. Consider two thermalizing channels  $\mathcal{T}^{(1)}$  and  $\mathcal{T}^{(2)}$  with Kraus operators  $\{E_i^{(1)}\}$  and  $\{E_j^{(2)}\}$ . If the two channels are applied in a definite order, the operator elements of the concatenated channel would be  $\{E_i^{(2)} E_j^{(1)}\}$  or  $\{E_i^{(1)} E_j^{(2)}\}$ , depending on which is applied first. Classically, the final state of the working substance remains the same if the two channels are equal, regardless of the causal order.

In the quantum realm, channels are allowed to be applied with ICO by introducing an ancilla, whose state controls the causal order of the applied channels. This composite quantum SWITCH [22, 33, 34] channel  $\mathcal{S}$  can be described by  $S_{ij} = |0\rangle\langle 0|_a \otimes E_i^{(2)} E_j^{(1)} + |1\rangle\langle 1|_a \otimes E_j^{(1)} E_i^{(2)}$ . Surprisingly, even if in the case of  $\mathcal{T}^{(1)} = \mathcal{T}^{(2)} = \mathcal{T}$ , the output state after applying  $\mathcal{S}$  can vary, depending on the projective measurement result on the ancilla. For instance, if we initialize the ancilla in an equal superposition state  $|\psi_a\rangle = |+\rangle = (|0\rangle + |1\rangle)/\sqrt{2}$ ,

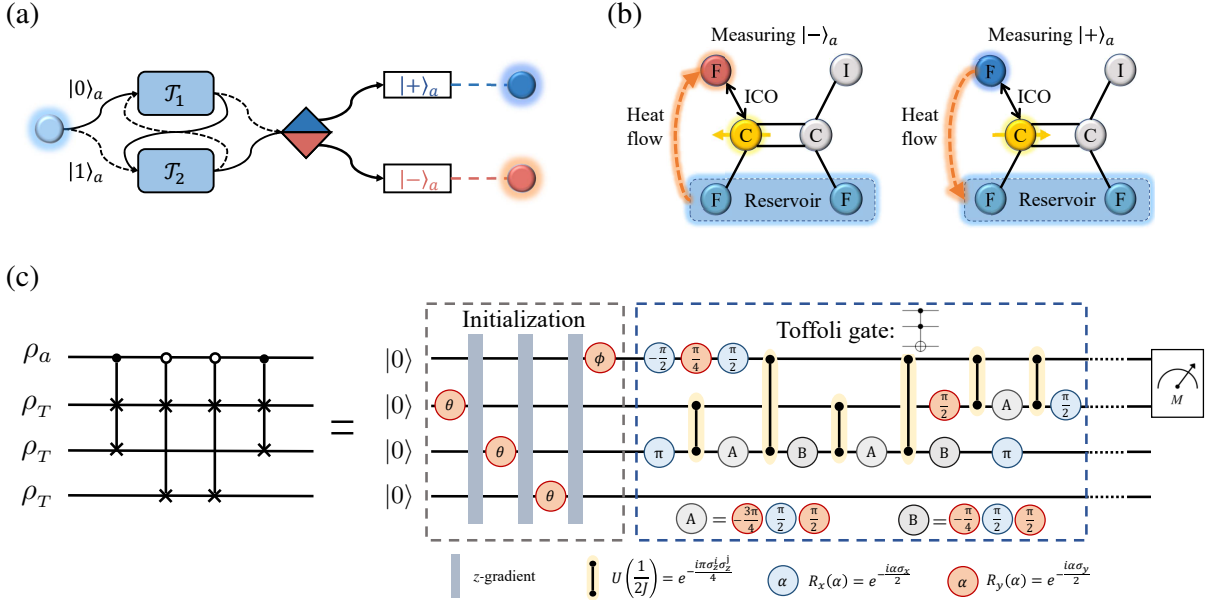


FIG. 1. (a) Quantum thermodynamics based on the ICO process. The two channels denoted by  $\mathcal{T}_1$  and  $\mathcal{T}_2$  represent two equal thermalizing channels, and the ball represents the working substance. In the beginning, its temperature is the same as that of the two reservoirs. After applying the quantum SWITCH, the ancilla is projected onto its  $|\pm\rangle_a$  subspace. When  $|- \rangle_a$  is detected, the heat transfers from the reservoirs to the working substance so that the system is heated (marked by red). Otherwise, the working substance is cooled (marked by blue). (b) Implementation of the ICO process on nuclear spins. In the sample  $\text{C}_2\text{F}_3\text{I}$ , we use the  $^{13}\text{C}$  as the ancilla, the upper  $^{19}\text{F}$  as the working substance, and two residual  $^{19}\text{F}$  as reservoirs. The direction of heat flow depends on the projective measurement result of the ancilla. Explicitly, heat transfers from (to) the reservoir to (from) the working system when the ancilla is measured  $|- \rangle_a$  ( $|+ \rangle_a$ ), respectively. (c) Quantum circuit and the relevant pulse sequence to implement the quantum SWITCH of thermalizing channels. The first qubit  $^{13}\text{C}$  is the ancilla, the second  $^{19}\text{F}$  is the working substance, and the last two  $^{19}\text{F}$  spins are used to imitate the effect of reservoirs. Each control-SWAP gate can be decomposed into three Toffoli gates. The pulse sequence shows the initialization of the system and the implementation of the first Toffoli gate.

the output after the quantum SWITCH operation will be

$$\begin{aligned} \mathcal{S}(\mathcal{T}, \mathcal{T})(\rho_a \otimes \rho) &= \frac{1}{2}(|0\rangle\langle 0|_a + |1\rangle\langle 1|_a) \otimes \rho_T \\ &+ \frac{1}{2}(|0\rangle\langle 1|_a + |1\rangle\langle 0|_a) \otimes \rho_T \rho \rho_T, \end{aligned} \quad (1)$$

where  $\rho_a = |\psi_a\rangle\langle\psi_a|$  and  $\rho_T = e^{-H/k_B T}$  is the thermal equilibrium state at temperature  $T$  with a two-level Hamiltonian  $H = \delta|e\rangle\langle e|$ . Here,  $\delta$  is the energy of the excited state of the system  $|e\rangle$ . If the ancilla is now measured in the computational basis, the system will be in the thermal state  $\rho_T$ , *i.e.*, the classical case. However, if it is measured in the  $\{|+\rangle_a, |-\rangle_a\}$  basis, the final state will be

$$\rho_{\pm} =_a \langle \pm | \mathcal{S}(\rho_a \otimes \rho) | \pm \rangle_a / P_{\pm} = \frac{\rho_T \pm \rho_T \rho \rho_T}{2P_{\pm}} \quad (2)$$

with the probability  $P_{\pm} = \text{Tr}[(\rho_T \pm \rho_T \rho \rho_T)/2]$ . In other words, the effective temperature of the final state can be higher or lower than  $T$  depending on the measurement result, as illustrated in Fig. 1(a). Even if we set the initial state  $\rho$ 's temperature as  $T$  – the same as that of the reservoirs – the final temperature can still vary. The key ingredient for this spooky phenomenon is that the Kraus operators of thermalizing channels do not commute with each other.

*Realizing the ICO process.* – The quantum SWITCH channel in Eq. (1) can be realized by a unitary quantum circuit as shown in the left of Fig. 1(c) [21]. In this circuit, the first qubit is assigned as the ancilla, the second as the working substance, and the last two in thermal equilibrium state  $\rho_T$  as two reservoirs.

In experiment, we use the four nuclei in  $^{13}\text{C}$ -iodotrifluoroethylene ( $\text{C}_2\text{F}_3\text{I}$ ) [35–37] dissolved in acetone-d6 to realize the ICO process, as shown in Fig. 1(b). The four nuclei represented by colorful balls are assigned as the four qubits, where the  $^{13}\text{C}$  (yellow),  $^{19}\text{F}$  (red and blue), and two residual  $^{19}\text{F}$  (cyan) are used as the ancilla, working substance, and reservoirs, respectively. Experiments are conducted at room temperature on a Bruker AVANCE 600 MHz NMR spectrometer equipped with a cryogenic probe. The natural Hamiltonian of the system reads  $\mathcal{H}_{\text{NMR}} = -\sum_{i=1}^4 \omega_i \sigma_z^i / 2 + \sum_{i < j} \pi J_{ij} 2\sigma_z^i \sigma_z^j / 2$ , where  $\omega_i / 2\pi$  is the Larmor frequency of the  $i$ -th spin, and  $J_{ij}$  is the scalar coupling between the  $i$ -th and  $j$ -th spins. All nuclear spins can be coherently controlled with high fidelity by radio-frequency pulses in the  $x$ - $y$  plane. The parameters of the sample are listed in the Supplemental Information [38].

The whole system starts at  $\rho_0 = \rho_a \otimes \rho_T \otimes \rho_T \otimes \rho_T$ . Here, we have fixed the initial effective temperature of the working substance as  $T$  – the same as that of the reser-

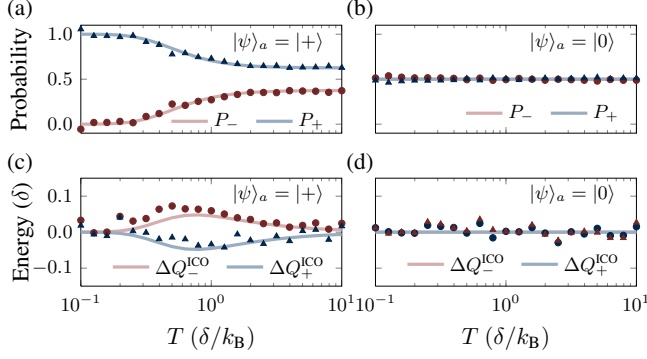


FIG. 2. (a-b) Probabilities  $P_{\pm}$  of measuring the ancilla in the  $|\pm\rangle$  basis. The ancilla is initialized in an (a) equal superposition state  $|+\rangle$  and (b)  $|0\rangle$ , respectively. Triangles and dots are experimental results, and solid lines are theoretical predictions. (c-d) Heat transfer between the working substance and reservoirs by measuring the ancilla in the  $|\pm\rangle$  basis, when the ancillary qubit is initialized in (c)  $|+\rangle$  and (d)  $|0\rangle$ , respectively.

voirs. This setting can fully exhibit the spooky action of the ICO process: even if the working substance and reservoirs have exactly the same starting temperature, the working substance can be warmed up or cooled down non-classically. For  $\rho_0$  initialization, we first apply a line-selective method [37] to create the pure state  $|0000\rangle$  [39]. Then, as shown in Fig. 1(c), we consequently apply three single-qubit rotations  $R_y(\theta) = e^{-i\sigma_y\theta/2}$  with  $\theta = \arccos(\rho_T^{(1,1)} - \rho_T^{(2,2)})$ , and three gradient-field pulses which destroy unwanted transverse terms. The working substance and reservoirs are all prepared at  $\rho_T$  now. Finally, an additional single-qubit rotation  $R_y(\phi)$  is applied on the ancillary qubit to create its superposition  $|\psi_a\rangle = \cos\frac{\phi}{2}|0\rangle + \sin\frac{\phi}{2}|1\rangle$ . Obviously, when  $\phi = 0$ , the ancilla is  $|\psi_a\rangle = |0\rangle$  like a classical case, and when  $\phi = \pi/2$ , the ancilla is  $|\psi_a\rangle = |+\rangle$  of maximal quantum superposition.

The quantum SWITCH operation is decomposed by a concatenation of control pulses and free Hamiltonian evolutions in experiment, as shown in Fig. 1(c). Since each control-SWAP gate can be decomposed into three Toffoli gates [32], we just plot the complete pulse sequence of the first Toffoli gate as an example. Then, we utilize the sequence compiler to reduce its complexity and gradient engineering optimization [40] to improve the control accuracy. The final shaped pulse after optimization is 25 ms with a simulated fidelity above 0.995. For readout, we perform two-qubit tomography [41, 42] on the ancilla and work substance [38], and reconstruct the experimental output state  $\rho_e$ . We compute the fidelity between  $\rho_e$  and the relevant theoretical prediction for all initial states. The fidelities are always over 0.96, indicating the well performance of the ICO process.

*Results of the ICO process.* – The first quantity from experimental investigation is the probability of projecting the ancilla to  $|\pm\rangle_a$ , which is  $P_{\pm} = \text{Tr}_a(\pm|\rho_e|\pm\rangle_a)$ . This important quantity reflects the success probability for particular heat flow direction. We fix the ancilla state  $|\psi_a\rangle$ , and vary the

temperature  $T$  of the working substance and two reservoirs. The results are shown in Fig. 2(a) and 2(b), where  $|\psi_a\rangle$  is  $|+\rangle$  and  $|0\rangle$ , respectively. Fig. 2(a) is the standard ICO process, where  $P_{\pm}$  vary against temperature  $T$ . When temperature goes lower, more remarkable quantum effect emerges as it is more possible to measure  $|+\rangle$  on the ancilla, which is related to a heat-up of the working substance. For higher temperatures,  $P_+$  and  $P_-$  eventually achieve stable values of 0.63 and 0.37, respectively. In Fig. 2(b), the input  $|\psi_a\rangle = |0\rangle$  means a classical situation. Not surprisingly, no differences are observed for measuring the ancilla in the  $|\pm\rangle$  basis. For other input states  $|\psi_a\rangle = \cos\frac{\phi}{2}|0\rangle + \sin\frac{\phi}{2}|1\rangle$  with unbalanced superpositions, the results are placed in the Supplemental Information [38].

The second important quantity is the amount of heat transfer between the working substance and reservoirs. In the ICO process, the average heat exchange can be defined as

$$\Delta Q_{\pm}^{\text{ICO}} = P_{\pm}[\text{Tr}(\rho_{\pm}H) - \text{Tr}(\rho_T H)], \quad (3)$$

where  $\rho_{\pm} = {}_a\langle\pm|\rho_e|\pm\rangle_a/P_{\pm}$  are the final states of the working substance when the ancilla is projected onto  $|\pm\rangle$ . The results are shown in Fig. 2(c) and 2(d) for the ICO and classical case, respectively. As expected, nonzero heat flow only occurs in the ICO process. Measuring  $|+\rangle_a$  indicates heat transfer from the working substance to reservoirs, which can thus be used to construct heat engines. On the contrary, the heat flow reverses which provides resources to construct quantum refrigerators. Due to the conservation of energy, the amount of heat transfer must equal for the heat-up and cool-down processes, *i.e.*,  $\Delta Q_{+}^{\text{ICO}} + \Delta Q_{-}^{\text{ICO}} = 0$ . Nevertheless, maximal heat flow happens at  $T = 0.8\delta/k_B$ .

*Realizing the ICO refrigerator.* – As shown above, the ICO process can be used to construct quantum heat engines or refrigerators. Here, we demonstrate a quantum cooling cycle driven by ICO in experiment, and study its efficiency by measuring the work consumption and the heat extracted from the cold reservoirs.

An ICO refrigerator consists of four strokes as shown in Fig. 3: (i) ICO process where projective measurement of the ancilla can be repeated. A Maxwell's demon allows the working substance to continue the cycle if  $|-\rangle_a$  is measured; (ii) classical heat exchange with the high-temperature reservoir and heat rejection; (iii) classical thermal contact with the low-temperature reservoir and heat rejection; (iv) initialization of the ancilla and erasure of the Maxwell's demon's memory. To evaluate the efficiency of the ICO refrigerator, we need to measure the heat energy extracted from the cold reservoir to the heat bath  $\Delta Q_C$  (what we want), and the work consumption  $W$  (what we pay for) in a cycle.

Assuming that all thermalizations are isochoric, the consumption of work only happens in stroke (iv), *i.e.*, when the demon's memory is erased. The expected work expenditure to reset the memory in contact with a resetting reservoir of temperature  $T_R$  is  $W = k_B T_R S$ . Here,  $S = -(P_- \ln P_- + P_+ \ln P_+)$  is the Shannon entropy of the demon's memory, where  $P_{\pm}$  is the probability of projecting the

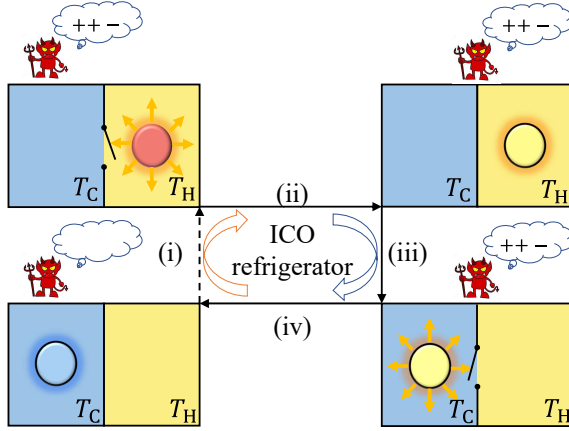


FIG. 3. Four-stroke ICO refrigerator cycle, which consists of two quantum stages (i) and (iv), and two classical heat exchange stages (ii) and (iii). After the ICO process (i), the Maxwell's demon measures the ancilla. The cycle continues only when the demon reads  $|-\rangle_a$ . Strokes (ii) and (iii) are thermal contacts with the hot and cold reservoirs, respectively. The last stroke (iv) reinitializes the working substance and erases the demon's memory.

ancilla qubit to  $|\pm\rangle_a$ . In experiment, we consider a constant resetting reservoir with  $T_R = \Delta/k_B$ , and the experimental work cost is given in Fig. 4(a) by blue dots. Clearly, the work consumption  $W$  increases as the cold reservoir's temperature  $T_C$  goes higher. The energy flow during strokes (i) - (iii) is in the form of heat exchange. Denoting the heat exchange of the working substance in the  $i$ -th stroke as  $\Delta Q_i$ , the net heat transfer of the cold reservoir in the whole cycle is  $\Delta Q_C = \Delta Q_2 = -(\Delta Q_1 + \Delta Q_3)$ , where the last equality comes from the conservation of the internal energy during the three strokes. The heat exchange in the second stroke is  $\Delta Q_2 = \text{Tr}(\rho_{-}H) - \text{Tr}(\rho_{T_H}H)$ , where  $\rho_{T_H}$  is the thermal equilibrium state of the hot reservoir. Therefore, to determine the net heat transfer  $\Delta Q_C$  from the cold reservoir, we just need to measure the released heat of the working substance in stroke (ii). This value depends on both the temperature of the hot reservoir  $T_H$  and cold reservoir  $T_C$ . It is well known that the maximal efficiency of a classical Carnot refrigerator approaches infinity when the temperature of the two reservoirs get closer. Here, we study the performance of the ICO refrigerator in an extreme case, *i.e.*,  $T_H = T_C$ . At the end of stroke (i), the four-qubit system is prepared into  $|-\rangle\langle-| \otimes \rho_{-} \otimes \rho_{T_H} \otimes \rho_{T_C}$ . We set  $T_H = T_C = T$  as a tunable parameter. Stroke (ii) is a thermal contact between the working substance and the hot reservoir, which can be simulated by a SWAP operation between qubits 2 and 3. We perform quantum state tomography on the working substance, yielding its internal energy  $\text{Tr}(\rho_{T_H}^e H)$  in experiment. The heat transfer  $\Delta Q_C = \Delta Q_2$  can thus be calculated, combining with the measured  $\rho_{-}$  in the ICO process. The result is displayed with red triangles in Fig. 4(a), illustrating that  $\Delta Q_C$  decreases with the increase of  $T_C$ .

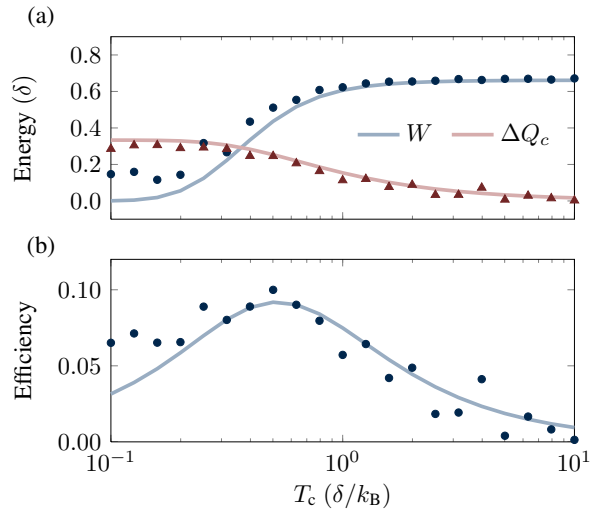


FIG. 4. (a) Work consumption  $W$  during a single ICO refrigeration cycle in theory (blue curve) and experiment (dots), and the heat transfer from the cold reservoir  $\Delta Q_C$  in theory (red curve) and experiment (triangles). The hot and cold reservoirs are set at the same temperature  $T_H = T_C$ . (b) Efficiency of the ICO refrigeration as a function of  $T_C$ . Solid lines and dots are theoretical and experimental results, respectively.

After measuring the work consumption  $W$  and heat transfer from the cold reservoir  $\Delta Q_C$ , we evaluate the efficiency of the ICO refrigerator at different reservoir temperatures. Unlike the classical case where the efficiency is simply  $\Delta Q_C/W$ , the ICO refrigerator is conditioned on whether the ancilla collapses to the  $|-\rangle_a$  subspace. While the work consumption always holds regardless of the measurement results, the success probability  $P_-$  must be taking into account when calculating the efficiency. Hence, the efficiency of the ICO refrigerator should be defined as

$$\eta = \frac{\text{what we want}}{\text{what we pay for}} = \frac{\Delta Q_C}{W/P_-}. \quad (4)$$

From the results shown in Fig. 4(b), we first see that  $\eta$  is not infinitely high at  $T_H = T_C$ , in contrary to the ideal Carnot refrigerator. Moreover, it varies with the temperature of the reservoir, and reaches an optimal value  $\eta_{\max} = 0.08$  at  $T_C = 0.6\delta/k_B$ . This result is genuinely distinct from what we have learned in the classical refrigeration, revealing unique properties of the ICO-based cooling.

*Discussion.* – We experimentally demonstrate that a quantum SWITCH of thermalizing channels supplies a new class of thermodynamic resources. Unlike a deterministic machine whose behavior can be characterized by a single thermodynamic cycle, the quantum machine driven by the ICO process is however not determinate. It can be a quantum refrigerator or heat engine depending on the projective measurement of the ancillary qubit. So, apart from the efficiency of a single thermodynamic cycle, the success probability is another critical parameter in evaluating the performance of the ICO thermo-

dynamics. In particular, we have shown two counterintuitive phenomena of the ICO process, which are nonexistent in the classical counterpart. One is that the working substance can be warmed up or cooled down even if it has the same temperature as that of reservoirs. The other is that the efficiency of the ICO refrigeration is bounded to small values at the extreme case. *i.e.*, the hot and cold reservoirs have the same temperature. Future efforts can be made by concatenating more or different thermalizing channels with quantum SWITCH to design quantum refrigerators with higher efficiency.

This work is supported by the National Key Research and Development Program of China (2019YFA0308100), National Natural Science Foundation of China (12075110, 11975117, 11905099, 11875159 and U1801661), Guangdong Basic and Applied Basic Research Foundation (2019A1515011383), Guangdong International Collaboration Program (2020A0505100001), Science, Technology and Innovation Commission of Shenzhen Municipality (ZDSYS20170303165926217, KQTD20190929173815000, JCYJ20200109140803865, JCYJ20170412152620376 and JCYJ20180302174036418), Pengcheng Scholars, Guangdong Innovative and Entrepreneurial Research Team Program (2019ZT08C044), and Guangdong Provincial Key Laboratory (2019B121203002).

---

\* These authors contributed equally to this work.

† [lij3@sustech.edu.cn](mailto:lij3@sustech.edu.cn)

‡ [xint@sustech.edu.cn](mailto:xint@sustech.edu.cn)

§ [ludw@sustech.edu.cn](mailto:ludw@sustech.edu.cn)

[1] G. J., M. M., and M. G., *Quantum Thermodynamics* (Springer, Berlin, 2004).

[2] T. D. Kieu, *Eur. J. Phys. D* **39**, 115 (2006).

[3] T. D. Kieu, *Phys. Rev. Lett.* **93**, 140403 (2004).

[4] H. T. Quan, P. Zhang, and C. P. Sun, *Phys. Rev. E* **72**, 056110 (2005).

[5] Y. A. Cengel and M. A. Boles, *Thermodynamics: An Engineering Approach 6th Editon (SI Units)* (The McGraw-Hill Companies, Inc., New York, 2007).

[6] R. Kosloff, *Entropy* **15**, 2100 (2013).

[7] M. Campisi, P. Hänggi, and P. Talkner, *Rev. Mod. Phys.* **83**, 771 (2011).

[8] M. Esposito, U. Harbola, and S. Mukamel, *Rev. Mod. Phys.* **81**, 1665 (2009).

[9] D. Kondepudi and I. Prigogine, *Modern thermodynamics: from heat engines to dissipative structures* (John Wiley & Sons, 2014).

[10] J. P. Dowling and G. J. Milburn, *Philos. Trans. Royal Soc. A* **361**, 1655 (2003).

[11] K. Micadei, J. P. Peterson, A. M. Souza, R. S. Sarthour, I. S. Oliveira, G. T. Landi, T. B. Batalhão, R. M. Serra, and E. Lutz, *Nat. Commun.* **10**, 1 (2019).

[12] J. P. Peterson, T. B. Batalhão, M. Herrera, A. M. Souza, R. S. Sarthour, I. S. Oliveira, and R. M. Serra, *Phys. Rev. Lett.* **123**, 240601 (2019).

[13] D. Gelbwaser-Klimovsky, W. Niedenzu, and G. Kurizki, in *Advances In Atomic, Molecular, and Optical Physics*, Vol. 64 (Elsevier, 2015) pp. 329–407.

[14] P. A. Camati, J. F. Santos, and R. M. Serra, *Phys. Rev. A* **99**, 062103 (2019).

[15] I. Georgescu and F. Nori, *Phys. World* **25**, 16 (2012).

[16] W. L. Ribeiro, G. T. Landi, and F. L. Semião, *Am J Phys* **84**, 948 (2016).

[17] L. Jaeger, *The Second Quantum Revolution* (Springer, 2018).

[18] P. A. Camati, J. F. G. Santos, and R. M. Serra, *Phys. Rev. A* **102**, 012217 (2020).

[19] K. Zawadzki, R. M. Serra, and I. D’Amico, *Phys. Rev. Res.* **2**, 033167 (2020).

[20] L. Szilard, *Z. Angew. Phys.* **53**, 840 (1929).

[21] D. Felce and V. Vedral, *Phys. Rev. Lett.* **125**, 070603 (2020).

[22] G. Chiribella, G. M. D’Ariano, P. Perinotti, and B. Valiron, *Phys. Rev. A* **88**, 022318 (2013).

[23] O. Oreshkov, F. Costa, and Č. Brukner, *Nat. Commun.* **3**, 1 (2012).

[24] M. Araújo, F. Costa, and i. c. v. Brukner, *Phys. Rev. Lett.* **113**, 250402 (2014).

[25] G. Rubino, L. A. Rozema, A. Feix, M. Araújo, J. M. Zeuner, L. M. Procopio, Č. Brukner, and P. Walther, *Sci. Adv.* **3**, e1602589 (2017).

[26] K. Wei, N. Tischler, S.-R. Zhao, Y.-H. Li, J. M. Arrazola, Y. Liu, W. Zhang, H. Li, L. You, Z. Wang, Y.-A. Chen, B. C. Sanders, Q. Zhang, G. J. Pryde, F. Xu, and J.-W. Pan, *Phys. Rev. Lett.* **122**, 120504 (2019).

[27] X. Zhao, Y. Yang, and G. Chiribella, *Phys. Rev. Lett.* **124**, 190503 (2020).

[28] M. Frey, *Quantum Inf. Process.* **18**, 96 (2019).

[29] D. Ebler, S. Salek, and G. Chiribella, *Phys. Rev. Lett.* **120**, 120502 (2018).

[30] Y. Guo, X.-M. Hu, Z.-B. Hou, H. Cao, J.-M. Cui, B.-H. Liu, Y.-F. Huang, C.-F. Li, G.-C. Guo, and G. Chiribella, *Phys. Rev. Lett.* **124**, 030502 (2020).

[31] T. Xin, Y. Li, Y.-a. Fan, X. Zhu, Y. Zhang, X. Nie, J. Li, Q. Liu, and D. Lu, *Phys. Rev. Lett.* **125**, 090502 (2020).

[32] M. A. Nielsen and I. Chuang, *Quantum computation and quantum information* (American Association of Physics Teachers, 2002).

[33] L. M. Procopio, A. Moqanaki, M. Araújo, F. Costa, I. A. Calafell, E. G. Dowd, D. R. Hamel, L. A. Rozema, Č. Brukner, and P. Walther, *Nat. Commun.* **6**, 1 (2015).

[34] P. A. Guérin, A. Feix, M. Araújo, and i. c. v. Brukner, *Phys. Rev. Lett.* **117**, 100502 (2016).

[35] J. Li, R. Fan, H. Wang, B. Ye, B. Zeng, H. Zhai, X. Peng, and J. Du, *Phys. Rev. X* **7**, 031011 (2017).

[36] H. Wang, S. Wei, C. Zheng, X. Kong, J. Wen, X. Nie, J. Li, D. Lu, and T. Xin, *Phys. Rev. A* **102**, 012610 (2020).

[37] X. Nie, B.-B. Wei, X. Chen, Z. Zhang, X. Zhao, C. Qiu, Y. Tian, Y. Ji, T. Xin, D. Lu, and J. Li, *Phys. Rev. Lett.* **124**, 250601 (2020).

[38] See Supplemental Material for more details.

[39] The system is actually in a pseudo-pure state, but its dynamics is the same as that of a pure state. More details in Supplemental Information.

[40] N. Khaneja, T. Reiss, C. Kehlet, T. Schulte-Herbrüggen, and S. J. Glaser, *J. Magn. Reson.* **172**, 296 (2005).

[41] D. Lu, T. Xin, N. Yu, Z. Ji, J. Chen, G. Long, J. Baugh, X. Peng, B. Zeng, and R. Laflamme, *Phys. Rev. Lett.* **116**, 230501 (2016).

[42] T. Xin, D. Lu, J. Klassen, N. Yu, Z. Ji, J. Chen, X. Ma, G. Long, B. Zeng, and R. Laflamme, *Phys. Rev. Lett.* **118**, 020401 (2017).